2009

Oxygen and hydrogen isotope fractionation in serpentine–water and talc–water systems from 250 to 450°C MPa

Peter Saccocia
Bridgewater State College, psaccocia@bridgew.edu

J. S. Seewald

W. C. Shanks III

Available online at www.sciencedirect.com
ScienceDirect
Geochimica et Cosmochimica Acta 73 (2009) 6789–6804
Geochimica et Cosmochimica Acta
www.elsevier.com/locate/gca

Oxygen and hydrogen isotope fractionation in serpentine–water and talc–water systems from 250 to 450 °C, 50 MPa

Peter J. Saccocia [a,*], Jeffrey S. Seewald [b], Wayne C. Shanks III [c]

[a] Department of Earth Sciences, Bridgewater State College, Bridgewater, MA 02325, USA
[b] Department of Marine Chemistry and Geochemistry, Woods Hole Oceanographic Institution, Woods Hole, MA 02543, USA
[c] United States Geological Survey, Denver Federal Center, Denver, CO 80225, USA

Received 6 March 2009; accepted in revised form 23 July 2009; available online 12 August 2009

Abstract

Oxygen and hydrogen isotope fractionation factors in the talc–water and serpentine–water systems have been determined by laboratory experiment from 250 to 450 °C at 50 MPa using the partial exchange technique. Talc was synthesized from brucite + quartz, resulting in nearly 100% exchange during reaction at 350 and 450 °C. For serpentine, D–H exchange was much more rapid than ^{18}O–^{16}O exchange when natural chrysotile fibers were employed in the initial charge. In experiments with lizardite as the starting charge, recrystallization to chrysotile enhanced the rate of ^{18}O–^{16}O exchange with the coexisting aqueous phase. Oxygen isotope fractionation factors in both the talc–water and serpentine–water systems decrease with increasing temperature and can be described from 250 to 450 °C by the relationships: $1000 \ln \alpha^{^{18}O-^{16}O}_{talc-water} = 11.70 \times 10^6/T^2 - 25.49 \times 10^3/T + 12.48$ and $1000 \ln \alpha^{^{18}O-^{16}O}_{serpentine-water} = 3.49 \times 10^6/T^2 - 9.48$ where T is temperature in Kelvin. Over the same temperature interval at 50 MPa, talc–water D–H fractionation is only weakly dependent on temperature, similar to brucite and chlorite, and can be described by the equation: $1000 \ln \alpha^{D/H}_{talc-water} = 10.88 \times 10^6/T^2 - 41.52 \times 10^3/T + 5.61$ where T is temperature in Kelvin. Our D–H serpentine–water fractionation factors calibrated by experiment decrease with temperature and form a consistent trend with fractionation factors derived from lower temperature field calibrations. By regression of these data, we have refined and extended the D–H fractionation curve from 25 to 450 °C, 50 MPa as follows: $1000 \ln \alpha^{D-H}_{serpentine-water} = 3.436 \times 10^6/T^2 - 34.736 \times 10^3/T + 21.67$ where T is temperature in Kelvin. These new data should improve the application of D–H and ^{18}O–^{16}O isotopes to constrain the temperature and origin of hydrothermal fluids responsible for serpentine formation in a variety of geologic settings.

1. INTRODUCTION

The alteration of ultramafic rocks to serpentine, talc, and other secondary minerals in the oceanic crust at mid-ocean ridges is a globally important process with significant geochemical, geophysical, and biological implications. For example, this process affects the long-term global geochemical fluxes for many elements (Früh-Green et al., 2004), the rheological properties of the oceanic lithosphere, particularly at slow-spreading ridges (Mevel and Cannat, 1992; Escartin et al., 1997), and the magnetic, gravity, and seismic velocity signatures of oceanic crust and upper mantle (e.g. Kelso et al., 1996; Miller et al., 1996; Blackman et al., 1998; Hirth et al., 1998). Moreover, production of reducing, methane-rich fluids during serpentinization may help sustain a deep biosphere in the oceanic lithosphere (Kelley et al., 2001). As a consequence, there has been renewed interest in recent years to define better the physical and chemical conditions associated with serpentine formation. In this context, the stable isotope composition of serpentine, talc, and other hydrous silicates can be used to constrain the temperature, pressure, and origin of hydrothermal fluids associated with serpentine formation, provided that accurate D–H and ^{18}O–^{16}O mineral–water

* Corresponding author.
E-mail address: psaccocia@bridgew.edu (P.J. Saccocia).

0016-7037/$ - see front matter © 2009 Elsevier Ltd. All rights reserved.
doi:10.1016/j.gca.2009.07.036

fractionation factors for key secondary minerals are known.

Oxygen isotope fractionation factors in the talc–water and serpentine–water system can be predicted using semi-empirical models based on bond strength (Zheng, 1993, 1998; Savin and Lee, 1988) but the results have not been verified by laboratory experiments. For hydrogen isotopes, purely theoretical models to compute specific mineral–water fractionation factors for complex hydrous silicates as a function of both temperature and pressure have not yet been developed (Chacko et al., 2001). Moreover, hydrogen isotope fractionation in the talc–water system has never been calibrated by experiment. Wenner and Taylor (1973) proposed a field-based calibration of hydrogen isotope fractionation in the serpentine–water system that is in poor agreement with the experimental calibration of Sakai and Tsutsumi (1978). This discrepancy has profound implications for models of serpentinization in a wide range of geologic environments including mid-ocean ridges. Mineev and Grinenko (1996) proposed that this discrepancy can be attributed to the effect of pressure on hydrogen isotope fractionation, but details about their experimental approach are not clear.

The purpose of this paper is to present new experimental data for D–H and ^{18}O–^{16}O fractionation in the serpentine–water and talc–water systems from 250 to 450 °C, 50 MPa. More specifically, these data constrain and extend the temperature- and pressure-dependent D–H fractionation factors for serpentine–water and provide the first experimental calibration of talc–water isotope fractionation.

2. EXPERIMENTAL

2.1. Approach

The fractionation factor between mineral and fluid ($\alpha_{mineral–fluid}$) can be defined by:

$$\alpha_{mineral–fluid} = \frac{1 + \frac{\delta_{mineral}}{1000}}{1 + \frac{\delta_{fluid}}{1000}} \quad (1)$$

where $\delta_{mineral}$ and δ_{fluid} refer to the isotopic composition of coexisting mineral and fluid samples, respectively, in standard δ notation as follows:

$$\delta_{sample} = \frac{R_{sample} - R_{standard}}{R_{standard}} \times 1000 \quad (2)$$

In Eq. (2), R_{sample} and $R_{standard}$ refer to the D/H or $^{18}O/^{16}O$ ratio of the sample and standard, respectively. All δ values are reported in units of per mil (‰) relative to VSMOW.

The partial exchange technique (Northrop and Clayton, 1966; Suzuoki and Epstein, 1976) was used in this study to determine equilibrium mineral–water fractionation factors. This technique involves the use of companion runs, defined here as two experimental charges that are identical in every respect except for the isotopic composition of the initial fluids. In this study, the initial fluids were prepared to be either isotopically enriched or depleted relative to the solid charge. For a given fluid–mineral pair, the extent of isotopic exchange can be defined by the relationship:

$$\%\ \text{exchange} = \frac{\ln\alpha_i - \ln\alpha_f}{\ln\alpha_i - \ln\alpha_e} \times 1000 \quad (3)$$

where α_i, α_f and α_e refer to the initial, final, and equilibrium value of $\alpha_{mineral–fluid}$. Thus, if it is assumed that the percentage of exchange in companion capsules is equal, α_e can be solved from:

$$\frac{\ln\alpha_{i,enr} - \ln\alpha_{f,enr}}{\ln\alpha_{i,enr} - \ln\alpha_e} = \frac{\ln\alpha_{i,dep} - \ln\alpha_{f,dep}}{\ln\alpha_{i,dep} - \ln\alpha_e} \quad (4)$$

where subscripts "enr" and "dep" refer to companion runs with initial fluids that are isotopically enriched and depleted, respectively. Our experiments employed both stable and unstable initial mineral assemblages. Where unstable initial assemblages were employed, isotope exchange was driven by extensive dissolution and recrystallization, which was equal, by design, in companion runs. This reaction process forces isotope exchange between solid and fluid to proceed from the same direction relative to the equilibrium distribution of isotopes, regardless of the initial isotopic composition of the fluid. Consequently, Eq. (4) can be applied to any mineral–fluid system, even those where the initial isotopic fractionation of the mineral–fluid pairs did not bracket the final equilibrium value, as long as it is reasonable to assume that the percent exchange (degree of recrystallization) is equal in companion runs. Ultimately, this approach involves an algebraic system that can be solved because the number of equations equals the number of unknowns.

2.2. Starting materials

For the experiments involving talc, two different starting materials were utilized (Fig. 1A and C). Talc from Balmat New York was purchased from Wards Natural Science, Inc. The composition of this specimen is $Mg_{3.18}Fe_{.01}Al_{.01}Si_{3.81}O_{10}(OH)_2$ and was determined by inductively coupled plasma mass spectrometry (ICPMS) following dissolution of a solid bead created by the lithium metaborate fusion technique. X-ray diffraction (XRD) analyses did not detect other minerals. Talc was also synthesized during a separate series of isotope-exchange experiments from a stoichiometric mixture of fine-grained reagent grade brucite and natural euhedral quartz crystals that were crushed to a grain size of 20–30 μm. At the temperature and pressure conditions of these experiments, quartz + brucite is an unstable assemblage that reacts to form talc according to the reaction:

$$3Mg(OH)_{2(s)} + 4SiO_{2(s)} \rightarrow Mg_3Si_4O_10(OH)_{2(s)} + 2H_2O_{(l)}$$

XRD and scanning electron microscopy (SEM) analyses of run products indicate that this reaction was rapid, going to completion within 14 days at 450 °C.

Two natural serpentine samples were used in these experiments (Fig. 1E and G). Lizardite (1T polytype based on XRD analyses) collected by the Royal Ontario Museum (sample #M 19804) from a serpentinized Grenville marble was used for the experiments conducted at 250 and 350 °C. Microprobe analysis yielded the following composition: $Mg_{6.03}Fe_{.08}Al_{.01}Si_{3.99}O_{10}(OH)_8$, where Fe is in the +3 oxidation state based on Mössbauer analyses (O'Hanley

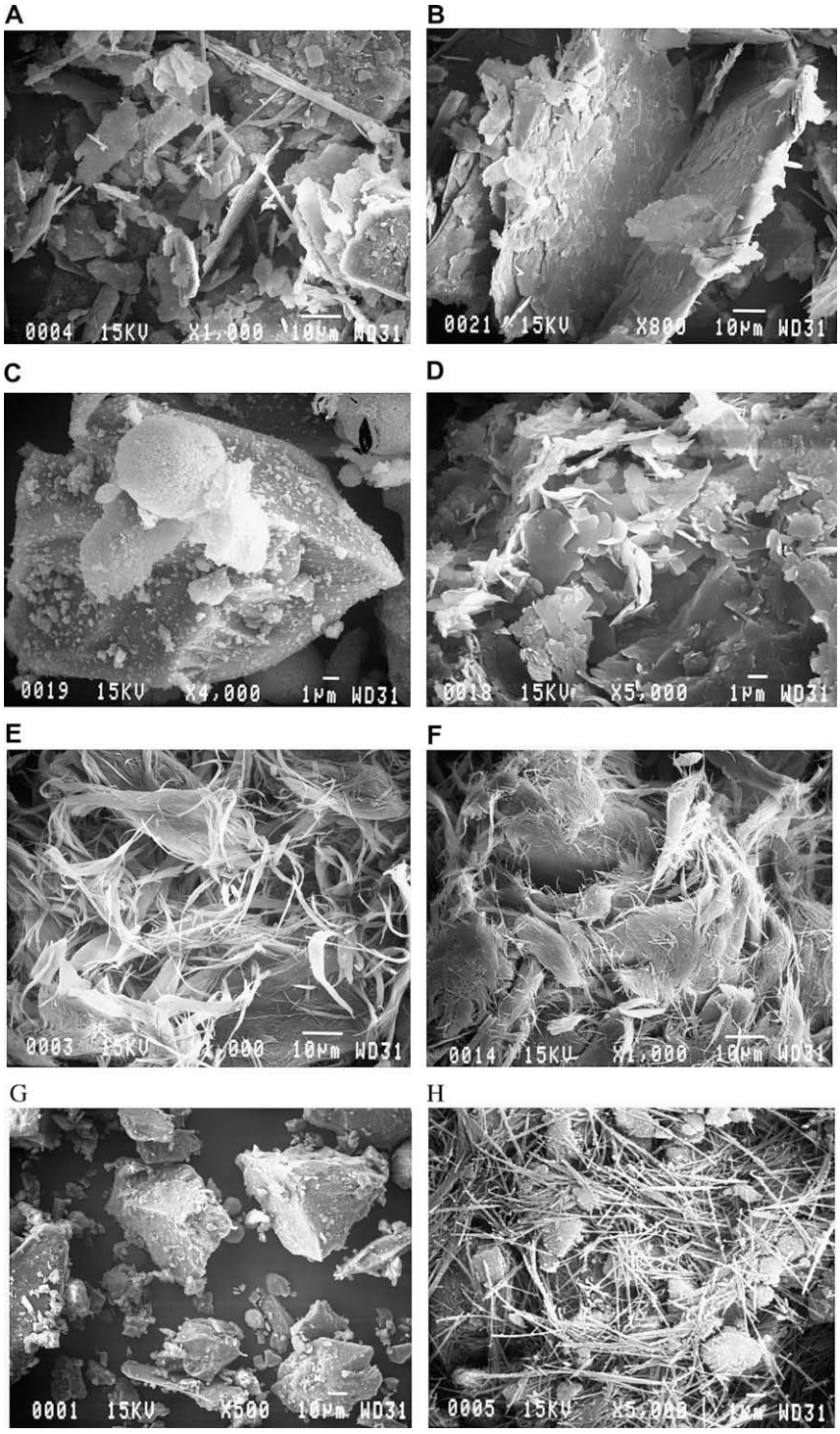

Fig. 1. SEM images of reactant and product phases. (A) Initial talc used in talc–water exchange experiments. (B) Talc crystals after reaction in talc–water exchange experiments. No significant difference in talc morphology is observed, indicating little or no recrystallization of the initial charge. (C) Initial quartz (subhedral crystal) + brucite (spherical mass) assemblage used in talc-synthesis experiments. (D) Euhedral talc crystals produced in synthesis experiments by recrystallization of the initial quartz + brucite assemblage. (E) Chrysotile fibers used as starting materials in exchange experiments between 250 and 450 °C. (F) Chrysotile fibers after reaction. No significant change in morphology is observed, indicating little or no recrystallization of the initial charge. (G) Lizardite used as starting material in exchange experiments at 250 and 350 °C. (H) Lizardite partially converting to chrysotile fibers in exchange experiments at 250 and 350 °C.

and Dyar, 1993). A chrysotile sample supplied by the Calidria Asbestos Company from a short-fiber chrysotile deposit in California was used for experiments conducted at 250, 350, and 450 °C. This material is 98% pure chrysotile

fiber; no other minerals were detected by XRD. The bulk composition of this sample is $Mg_{5.99}Ca_{.04}Fe_{.09}Al_{.02}Si_{3.83}O_{10}(OH)_8$, where all Fe is assumed to be in the +3 oxidation state. This was determined by ICPMS analysis following digestion of a solid bead produced by the lithium–metaborate fusion technique. Our choice of reactants for the serpentine experiments was guided by phase relations that suggest lizardite is more stable at lower temperatures compared to chrysotile (Berman, 1988).

All starting fluids were 3.0 wt.% NaCl solutions prepared from de-ionized water, reagent grade NaCl, and water isotopically enriched or depleted in D and ^{18}O. The NaCl was added to increase the solubility and reactivity of the hydrous silicates. The effect of added salt on mineral–water fractionation is minor ($\leqslant 0.1‰$ and $\leqslant 1.0‰$ for ^{18}O–^{16}O and D–H respectively) at the conditions of these experiments (Horita et al., 1995; Driesner and Seward, 2000).

2.3. Methods

Experiments were performed using flexible gold capsules (1 cm o.d., 0.13 mm wall thickness, 5 cm length, 4 ml internal volume) contained within steel pressure vessels. Gold capsules were welded at one end before loading solid (0.20 g) and fluid (1.25–1.50 g) reactants. The resulting fluid/solid mass ratios of 6.25–7.50 were sufficiently high so that any isotopic changes in the fluid would be insignificant, minimizing the potential for isotopic zonation in the solid products.

After loading the solid and fluid reactants, each gold capsule was purged with He to remove air before the open end was squeezed in a vice to create an initial seal. This seal was then welded while the capsule was submerged in liquid nitrogen to prevent heating of the capsule contents. The weight of the sealed capsule was then compared to the initial weight of the unsealed gold capsule plus the fluid and solid reactants. Sealed capsules that differed from the initial weight (before welding) by more than 1% were not used.

For each mineral–fluid system investigated at a given temperature, a total of six gold capsules were prepared. All capsules had identical solid reactants. Three capsules were loaded with isotopically enriched fluids and three were loaded with isotopically depleted fluids. Each pair of capsules with different initial fluids (enriched and depleted) was then placed in one of three different pressure vessels and all three pressure vessels were loaded into a single tube furnace. The internal pressure of each gold capsule was externally controlled at 50 MPa by pumping water into the pressure vessels. Temperature was monitored by a thermocouple inserted into a well at the back end of each pressure vessel that extended into the pressure fluid surrounding the gold capsules. To monitor temperature gradients, two additional thermocouples were attached along the exterior wall of each pressure vessel. The tube furnace containing the pressure vessels was heated to the desired temperature in less than 2 h while bleeding off excess pressure fluid. Using this apparatus, the temperature inside and along the entire length of each pressure vessel was controlled and known to ±2 °C.

The isotopic compositions of solid and fluid products were determined as a function of time by removing a single pressure vessel from the tube furnace at selected time intervals, without disturbing the temperature and pressure condition of the remaining vessels. This approach allowed us to adjust reaction times as needed depending on temperature and isotope exchange rates. Reaction times varied from 14 to 225 days.

During sampling, each pressure vessel was cooled to room temperature in less than 10 min by exposure to a cold gas stream followed by immersion in a chilled water bath. Because the solubility of both talc and serpentine increases with decreasing temperature and is extremely small in near neutral pH fluids used for this study (Saccocia and Seyfried, 1990), mineral precipitation cannot occur during quench. Mineral dissolution would be minor and have little or no measurable effect on the isotopic composition of the fluid and solid phases.

Immediately after cooling, cleaning, and weighing, each capsule was punctured with a hypodermic needle to transfer the fluid to a glass gas-tight syringe. The fluids were passed through a 0.22 μm syringe filter to remove particulates and sealed in a glass ampule for chemical analysis. The solids were dried at 40 °C prior to isotopic analyses and mineralogical characterization by XRD and SEM. Dissolved Cl was determined using ion chromatography. A decrease in Cl indicated that a capsule had leaked; all results from such a capsule were discarded.

Isotopic analyses were performed at the USGS in Denver using a Finnigan Mat 252 mass spectrometer. For H-isotopic analyses samples were heated in a vacuum overnight at 80 °C. Water was then liberated by heating in a Pt boat using an induction coil and converted to H_2 gas by reaction with either U or Zn (Godfrey, 1962). The oxygen isotopic composition of the solids was determined by the BrF_5 technique (Clayton and Mayeda, 1963). For the starting waters, the δD was determined by zinc reduction following the technique of Coleman et al. (1982) and the $\delta^{18}O$ was determined using the CO_2 equilibration method of O'Neil et al. (1975). Analytical precision for isotope analyses was ±0.2‰ and ±3‰ for $^{18}O/^{16}O$ and D/H, respectively. Because the experiments were conducted in a closed system with high fluid/solid mass ratios, changes in the isotopic composition of the starting fluids were less than the precision of our analytical techniques. The isotopic composition of the fluid after reaction was therefore calculated by material balance using the large measured changes in the isotopic composition of the solid phases.

3. RESULTS

Equilibrium fractionation factors (α_e) for all mineral–water pairs were calculated as a function of reaction progress using the partial exchange technique. Ideally, the resulting α_e values should not change with time if all assumptions inherent in the partial exchange technique are valid and uncertainties associated with the experimental design and analytical methods are nonexistent. Consequently, calculated values of α_e that do vary with time reflect the total uncertainty associated with this approach.

In the results reported here, we adopted the mean α_e value calculated from multiple samples as a function of time as being the most representative equilibrium mineral–water fractionation factor. This is a statistically conservative approach that places equal significance on the results from each sampling occasion. Accordingly, our reported uncertainties are equivalent to the standard deviation of α_e values computed for all samples in a given experiment. As an additional test, we propagated the analytical uncertainties associated with δD and $\delta^{18}O$ measurement of the solid products through Eqs. (3) and (4) for each sample. The uncertainty computed by this method was in excellent agreement with the standard deviation of α_e values for experiments with both low and high percents of isotope exchange. In those cases where differences were observed, the larger uncertainty was adopted.

3.1. Talc–water experiments

In one series of experiments, talc was reacted with isotopically enriched and depleted NaCl solutions at 250 and 350 °C (Table 1). At these conditions, oxygen isotope exchange was <7%, even after 223 days of reaction at 350 °C. The $\delta^{18}O$ of the initial talc changed by <1‰ during these runs, and consequently, mineral–water fractionation ($\Delta^{18}O_{talc-water}$) remained essentially unchanged in both the enriched and depleted companion capsules (Fig. 2A and B). SEM examination of the talc before and after reaction revealed little difference in morphology and perhaps only a slight increase in crystal size, indicating that talc recrystallizes slowly at these conditions (Fig. 1B). The lack of significant recrystallization and oxygen isotope exchange also indicates that volume diffusion must be slow at these temperatures, even with respect to oxygen in hydroxyl sites. As a consequence, these experiments could not be used to compute equilibrium oxygen isotope fractionation factors.

The δD of talc in these same experiments changed measurably after reaction with both the enriched and depleted waters (Table 1). These data indicate a more rapid exchange of hydrogen isotopes consistent with results from other exchange experiments involving hydrous silicates (Cole and Ohmoto, 1986). However, time-dependent talc–water fractionation ($\Delta D_{talc-water}$) in depleted and enriched companion runs failed to converge consistently with time, or in some cases, actually diverged with time (Fig. 2C and D). As a consequence, solving Eqs. (3) and (4) was not possible for some companion runs and yielded highly erratic results in others (Table 1), precluding the use of these data to define the equilibrium hydrogen isotope fractionation factor between talc and water.

3.2. Talc synthesis – water experiments

In a second series of experiments, we synthesized talc from brucite and quartz at temperatures between 250 and 450 °C. SEM observations revealed nearly complete conversion of brucite + quartz to talc after 14 days at 450 °C (Fig. 1C and D). Similar results were observed at 350 °C, although at 250 °C some of the initial reactants remained. XRD analyses of the reaction products showed intense basal reflections characteristic of talc.

The extent of oxygen and hydrogen isotope exchange was nearly 100% at 350 and 450 °C (Table 1). At 250 °C, the extent of exchange reached 55–77% for D–H and ^{18}O–^{16}O, respectively, reflecting slower recrystallization at this temperature. Site-specific exchange in the talc structure (*e.g.* oxygen within the hydroxyl group verses the silicon tetrahedron) could produce large uncertainties if the rate of isotope exchange between these different sites and water was not the same. Because these experiments were designed to force isotope exchange by recrystallizing the solid reactants, it is unlikely that this type of site-specific kinetic process influenced the talc–water fractionation factors reported here.

At 250 °C incomplete recrystallization of the initial reactants may contribute additional uncertainty to our reported fractionation factors if volume diffusion of oxygen and hydrogen isotopes between water and any remaining brucite and quartz was occurring. Saccocia et al. (1998) showed that oxygen and hydrogen isotope exchange in the brucite–water system at 250 °C, utilizing the same initial brucite sample, was driven by a rapid pulse of recrystallization with very little subsequent exchange for run times up to 210 days. This suggests that volume diffusion of oxygen and hydrogen between brucite and water is extremely slow at this low temperature. Similarly, oxygen isotope exchange between quartz and water at 250 °C is dominated by dissolution and recrystallization processes that precede much slower volume diffusion (Matthews et al. 1983). If these conclusions are correct, then fractionation factors for the talc–water system calculated here using the partial exchange technique should still be valid. The fact that $\Delta^{18}O_{talc-water}$ and $\Delta D_{talc-water}$ observed in the talc-synthesis experiments conducted at 250 °C varied systematically as a function of time (Fig. 3A and B) provides additional support for this conclusion. But other studies do show that hydrogen isotopes can diffuse rapidly through crystal structures (Cole and Ohmoto, 1986). Indeed, results reported here for experiments involving the incomplete recrystallization of lizardite to chrysotile (see below) suggest that volume diffusion of hydrogen isotopes may be occurring at temperatures as low as 250 °C. Thus, we cannot rule out complicating effects due to incomplete recrystallization processes in the talc-synthesis experiment at 250 °C. The reported uncertainties at this condition should therefore be considered minimum values.

The calculated extent of D–H exchange during talc synthesis at 350 °C exceeded 100% (Table 1), as shown by the cross-over of mineral–water fractionation values in the enriched and depleted companion runs (Fig. 3D). This, of course, is not possible and no anomalous run products were observed. We attribute this result to larger analytical and/or experimental uncertainties in the depleted companion capsules at 350 °C. In these runs, the measured δD of the talc decreased with time from an initial value of −74‰ to −97‰ after 70 days of reaction, but then increased to −85‰ after 225 days of reaction (Table 1). The resulting talc–water D–H fractionation values do not change in a systematic manner with time (Fig. 3D). In contrast, the δD of talc produced in the enriched companion runs exhibits a monotonic increase from −74 to −11‰ with reaction

Table 1
Hydrogen and oxygen isotope data for talc–water fractionation experiments.

Days	T (°C)	NaCl wt.%	Initial fluid enriched in D and ^{18}O						Initial fluid depleted in D and ^{18}O						D–H		^{18}O–^{16}O	
			Talc (grams)	Water (grams)	δD_{talc}	δD_{water}	$\delta^{18}O_{talc}$	$\delta^{18}O_{water}$	Talc (grams)	Water (grams)	δD_{talc}	δD_{water}	$\delta^{18}O_{talc}$	$\delta^{18}O_{water}$	$10^3 \ln \alpha_{talc-water}$	% ex	$10^3 \ln \alpha_{talc-water}$	% ex
Talc–salt water																		
0	250	3.0			−7	23	21.9	29.8			−7	−44	21.9	12.4				
27	250	3.0	0.2008	1.5320	−48	23	21.6	29.8	0.2001	1.5325	−48	−44	21.3	12.4	*	*	−24.7	2
118	250	3.0	0.2004	1.5275	−44	23	22.2	29.8	0.2005	1.5302	−47	−44	21.0	12.5	−848	5	−3.4	7
210	250	3.0	0.2003	1.5233	−63	23	22.4	29.8	0.2015	1.5316	−52	−44	21.2	12.5	307	−17	−0.6	7
Talc–salt water																		
0	350	3.0			−7	23	21.9	29.8			−7	−44	21.9	12.4				
31	350	3.0	0.1993	1.5316	−32	23	22.2	29.8	0.1996	1.4801	−47	−44	21.5	12.4	−140	23	−0.4	4
79	350	3.0	0.1996	1.5260	−43	23	22.6	29.7	0.2014	1.5270	−49	−44	21.3	12.4	−427	9	1.5	8
128	350	3.0	0.2007	1.5308	−49	23	22.5	29.8	0.2007	1.5222	−50	−44	21.3	12.4	−2812	2	0.8	7
223	350	3.0	0.2015	1.5006	−49	23	22.3	29.8	0.1998	1.5259	−80	−44	21.1	12.5	−118	49	−2	7
Talc synthesis																		
0	250	3.0			−74	23	9.8	29.8			−74	−44	9.8	12.4				
35	250	3.0	0.2001	1.5264	−45	23	27.3	28.5	0.1999	1.5321	−73	−44	15.8	11.9	−29	45	6.4	71
80	250	3.0	0.1771	1.5339	−42	23	27.6	28.6	0.1739	1.5324	−77	−44	16.2	12.0	−38	55	7.1	70
139	250	3.0	0.1922	1.5301			28.7	28.4	0.2070	1.5403			16.1	11.9			6.1	77
Talc synthesis																		
0	350	3.0			−74	23	9.8	29.8			−74	−44	9.8	12.4				
32	350	3.0	0.2060	1.5177	−32	23	28.3	28.3	0.2045	1.5209	−81	−44	13.8	12.1	−42	77	2.2	90
70	350	3.0	0.2073	1.5146	−22	23	25.5	28.5	0.2025	1.5189	−97	−44	13.0	12.1	−53	118	1.8	78
225	350	3.0	0.2027	1.5184	−11	23	28.3	28.3	0.2013	1.5201	−85	−44	13.0	12.2	−42	115	1.0	95
Talc synthesis																		
0	450	3.0			−74	23	9.8	29.8			−74	−44	9.8	12.4				
14	450	3.0	0.2073	1.2653	−9	22	26.9	28.2	0.2023	1.2507	−75	−44	11.7	12.2	−33	102	−0.4	96
30	450	3.0	Capsule	Leaked					0.2054	1.2550	−73		11.8					
45	450	3.0	0.2028	1.2697	−14	23	27.0	28.2	0.2071	1.2554	−71	−44	11.7	12.2	−28	88	−0.4	96

*Unable to solve.

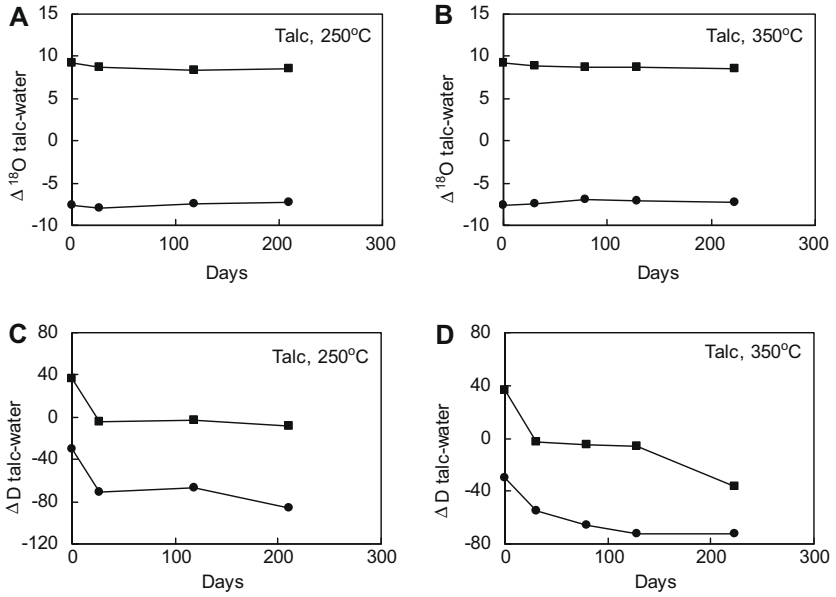

Fig. 2. Talc–water fractionation ($\delta_{mineral} - \delta_{water}$) versus experimental run-time for the reaction of talc and NaCl solutions at 250 and 350 °C. Individual graphs show data for companion runs involving isotopically enriched (circles) and depleted (squares) waters. Oxygen-isotope exchange was minimal (<7%), as evidenced by talc–water fractionation that were unchanged over time. Hydrogen isotope exchange was more significant but the time-dependent trends observed precluded retrieval of fractionation factors.

progress which is the expected result. Talc–water D–H fractionation in these runs increased regularly with time from an initial value of −100 to −33‰ at the termination of the experiment. This is consistent with a minimum value of −33‰ for the equilibrium D–H fractionation factor for talc at 350 °C. However, the observed cross-over in talc–water D–H fractionation precludes a more precise determination at this condition.

The starting isotopic composition of the companion runs with depleted water at 450 °C was close to equilibrium fractionation in the talc–water system. This is indicated by the small measured changes in the δD and $\delta^{18}O$ of the newly formed talc after recrystallization of the initial brucite–quartz assemblage (Table 1). It is important to note that companion runs with enriched water at 450 °C showed large changes in the isotopic composition of the solid charge, yielding mineral–water fractionation values that rapidly converged with those measured in the depleted companion runs (Fig. 3E and F), with resulting extents of exchange close to 100%. Thus, these runs provide good constraints on the equilibrium fractionation factors between talc and water.

Our results indicate that the talc–water oxygen isotope fractionation factor ($1000 \ln \alpha^{^{18}O\_^{16}O}_{talc-water}$) decreases from 6.5 ± 0.6‰ at 250 °C to −0.4 ± 0.2‰ at 450 °C (Table 3). The talc–water hydrogen isotope fractionation factor ($1000 \ln \alpha^{D/H}_{talc-water}$) is not highly dependent on temperature varying from −34 ± 7‰ at 250 °C to −31 ± 4‰ at 450 °C, 50 MPa (Table 3).

3.3. Chrysotile–water experiments

Chrysotile was reacted with NaCl solutions at 250, 350, and 450 °C for reaction times up to 225 days. Hydrogen isotopes exchanged more rapidly than oxygen isotopes in the chrysotile–water experiments (Table 2, Fig. 4). D–H exchange varied from 73% at 250 °C for run times up to 139 days, to 89% at 450 °C for run times up to 45 days. For ^{18}O–^{16}O, the amount of exchange varied from 6% at 250 °C to 19% at 450 °C. SEM examination of the chrysotile before and after the experiment revealed little difference in fiber morphology and little or no evidence for recrystallization (Fig. 1E and F). XRD analyses also revealed no change in chrysotile morphology after reaction. As a consequence, volume diffusion is the most likely mechanism for exchange in these experiments, consistent with the large difference in the calculated extents of exchange for oxygen and hydrogen.

Large changes were observed in time-dependent D–H chrysotile–water fractionation ($\Delta D_{chrysotile-water}$) in companion capsules from initial conditions that were as much as 60‰ above or below the equilibrium distribution of isotopes (Fig. 4B, D and F). The data at 450 °C are particularly consistent, with identical α_e values calculated at two different stages of reaction progress (Table 2). At lower temperature, the time-dependent results were less systematic, leading to larger uncertainties in the final α_e values. Our data show that $1000 \ln \alpha_e$ for D–H chrysotile–water fractionation increases with increasing temperature, ranging from −32 ± 15‰ at 250 °C to −20 ± 2‰ at 450 °C (Table 3).

Our ability to calculate $1000 \ln \alpha_e$ for ^{18}O–^{16}O chrysotile–water fractionation was precluded by low extents of isotope exchange (<10%) at 250 and 350 °C. At 450 °C, our data are consistent with a $1000 \ln \alpha_e$ value of −3.1 ± 1.3, although it should be emphasized that even at this relatively high temperature the extent of exchange was only 19%. Moreover, we are not able to evaluate the potential for differing rates of site-specific ^{18}O–^{16}O exchange in the

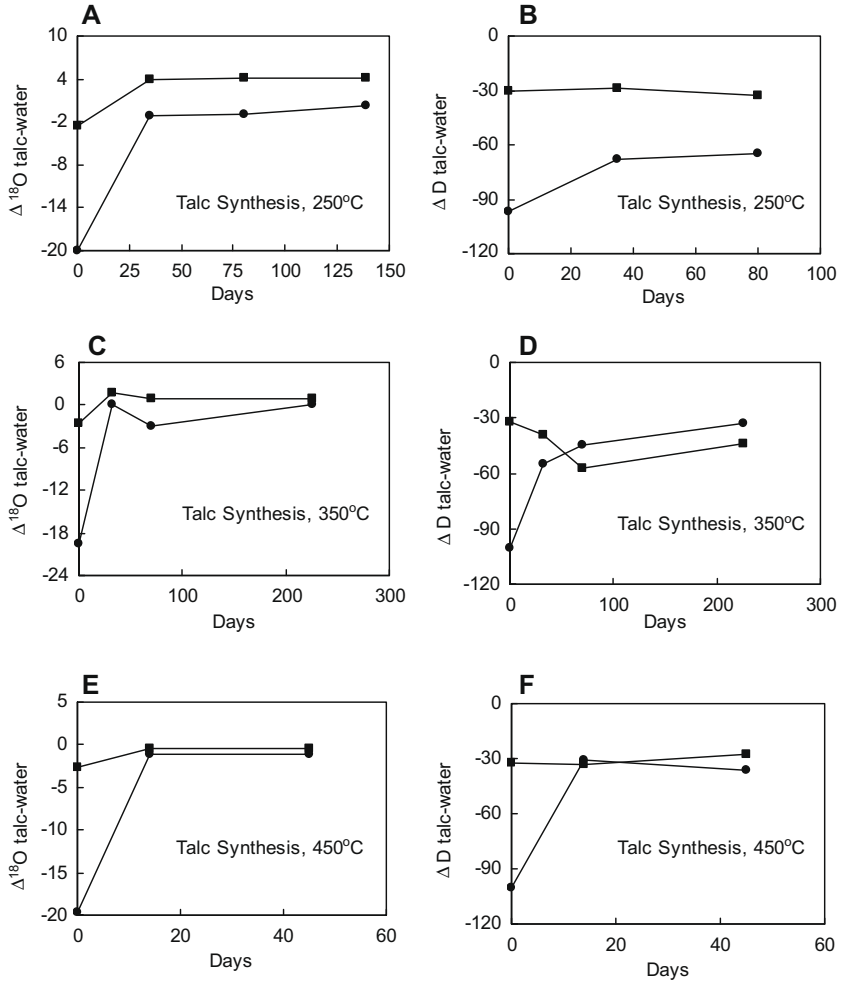

Fig. 3. Talc–water fractionation ($\delta_{mineral} - \delta_{water}$) versus experimental run-time for experiments in which talc was synthesized from brucite + quartz in NaCl solutions between 250 and 450 °C. Individual graphs show data for companion runs involving isotopically enriched (circles) and depleted (squares) waters. The extent of equilibration ranged from 55% at 250 °C to 100% at 450 °C.

chrysotile structure. Thus, the actual uncertainty associated with this value could be much greater.

3.4. Lizardite–water experiments

In the lizardite experiments at 250 and 350 °C, the starting lizardite partially converted to chrysotile fibers (Fig. 1G and H). This enhanced ^{18}O–^{16}O exchange relative to experiments in which chrysotile experienced little or no recrystallization. The extent of oxygen-isotope exchange varied from 17% at 250 °C to 82% at 350 °C (Table 2) and both experiments display systematic convergence of serpentine–water fractionation ($\Delta^{18}O_{serpentine-water}$) as a function of time in companion capsules (Fig. 5C and D). The implication of this result is that the observed exchange of oxygen isotopes must be a direct function of the extent of lizardite conversion to chrysotile. Based on these results, we compute 1000 ln α_e values for chrysotile–water ^{18}O–^{16}O fractionation of $3.1 \pm 1.2‰$ and $0.0 \pm 1.1‰$ at 250 and 350 °C, respectively (Table 3). When considered with the 450 °C data point from the chrysotile–water experiments, our results suggest that the ^{18}O–^{16}O fractionation factor for serpentine–water decreases with increasing temperature in a manner similar to talc. We are most confident in the reported fractionation factor at 350 °C because the high degree of lizardite recrystallization in this experiment facilitated more extensive isotope exchange (82%) compared to the lizardite and chrysotile experiments at 250 and 450 °C, respectively.

The δD of the solid products in the lizardite experiments suggests that multiple exchange processes due to the incomplete conversion lizardite to chrysotile may have controlled fractionation of hydrogen isotopes. D–H lizardite–water fractionation values ($\Delta D_{serpentine-water}$) for companion capsules decrease initially, and then slowly increase with continued reaction progress, but never converge toward a single value. This pattern is observed in both the 250 and 350 °C lizardite experiments (Fig. 5A and B) and precludes an equilibrium model for the time-dependent distribution of hydrogen isotopes between solid and fluid. A possible explanation is that two competing D–H exchange mechanisms were occurring. First, D–H exchange between the initial lizardite and the coexisting water by volume diffusion probably occurred given that lizardite was identified in

Table 2
Hydrogen and oxygen isotope data for serpentine–water fractionation experiments.

Days	T (°C)	NaCl (wt.%)	Initial fluid enriched in D and ^{18}O						Initial fluid depleted in D and ^{18}O						D–H		^{18}O–^{16}O	
			Serp. (grams)	Water (grams)	δD_{serp}	δD_{water}	$\delta^{18}O_{serp}$	$\delta^{18}O_{water}$	Serp. (grams)	Water (grams)	δD_{serp}	δD_{water}	$\delta^{18}O_{serp}$	$\delta^{18}O_{water}$	$10^3 \ln \alpha_{talc-water}$	% ex	$10^3 \ln \alpha_{talc-water}$	% ex
Lizardite–salt water																		
0	250	3.0			−56	−18	8.9	22.6			−56	−125	8.9	−53.0				
27	250	3.0	0.2012	1.5264	−73	−18	10.8	22.4	0.2005	1.5294	−136	−124	1.7	−52.4	−69	62	2.4	13
70	250	3.0	0.2000	1.5344	−81	−18	11.1	22.4	0.1998	1.5272	−146	−123	1.3	−52.4	−82	65	3.6	14
118	250	3.0	0.2003	1.5298	−74	−18	11.1	22.4	0.2004	1.4875	−145	−123	0.6	−52.3	−67	70	2.4	15
210	250	3.0	0.2000	1.5269	−58	−18	11.6	22.4	0.2010	1.5333	−117	−124	−0.3	−52.3	−43	57	3.8	17
Lizardite–salt water																		
0	350	3.0			−56	−18	8.9	22.6			−56	−125	8.9	−53.0				
31	350	3.0	0.2011	1.5338	−61	−18	13.4	22.2	0.2010	1.5257	−134	−124	−11.8	−51.3	−47	71	0.0	35
79	350	3.0	0.1998	1.5237	−72	−18	14.8	22.1	0.2002	1.5296	−138	−124	−18.3	−50.9	−66	65	0.0	47
128	350	3.0	0.2000	1.5348	−75	−18	17.6	21.9	0.2011	1.5312	−141	−124	−26.6	−50.2	−71	65	1.3	63
223	350	3.0	0.1996	1.4862	−58	−18	18.3	21.8	0.2007	1.5377	−127	−124	−39.3	−49.2	−43	67	−1.3	82
Chrysotile–salt water																		
0	250	3.0			−93	−18	8.7	22.6			−93	−125	8.7	−53.0				
35	250	3.0	0.2015	1.5321	−71	−18	9.1	22.6	0.1999	1.5348	−121	−125	5.9	−52.8	−30	48	−8.7	4
80	250	3.0	0.2069	1.5386	−84	−18	9.4	22.6	0.2037	1.5465	−118	−125	5.1	−52.7	−48	33	−4.6	6
139	250	3.0	0.1984	1.5399	−53	−19	9.6	22.6	0.2024	1.5303	−128	−124	5.3	−52.7	−19	73	−1.1	6
Chrysotile–salt water																		
0	350	3.0			−93	−18	8.7	22.6			−93	−125	8.7	−53.0				
32	350	3.0	0.2047	1.6615	−57	−19	9.6	22.5	0.2053	1.5121	−131	−124	3.7	−52.6	−25	72	−2.1	8
70	350	3.0	0.2055	1.5188	−54	−19	10.4	22.5	0.2047	1.5134	−135	−124	3.2	−52.6	−25	79	4.3	10
225	350	3.0	0.2023	1.5176	−60	−19	9.6	22.5	0.2058	1.5090	−149	−124	2.8	−52.5	−38	88	−3.6	10
Chrysotile–salt water																		
0	450	3.0			−93	−18	8.7	22.6			−93	−125	8.7	−53.0				
14	450	3.0	0.2058	1.2631	−53	−19	10.4	22.4	0.2021	1.2595	−129	−124	−1.0	−52.1	−20	74	−2.3	16
30	450	3.0	0.2064	1.2629	−46	−19	10.1	22.5	0.2057	1.2554	−135	−124	−1.4	−52.0	−20	87	−4.4	17
45	450	3.0	0.2040	1.2738	−45	−19	10.6	22.4	0.2029	1.2613	−136	−124	−2.4	−51.9	−20	89	−2.6	19

the solid products (i.e. incomplete conversion to chrysotile). A similar D–H exchange mechanism was inferred from the results of the talc–water and chrysotile–water experiments where recystallization was minimal. Second, D–H fractionation must have occurred between the water and the chrysotile fibers formed by progressive conversion of lizardite. Thus, the combination of these two simultaneous processes operating at different rates and involving two different phases, may have prevented the hydrogen isotopes from reaching equilibrium between the solid products and coexisting water as a function of time. In contrast, the ^{18}O–^{16}O serpentine–water fractionation values ($\Delta^{18}O_{serpentine-water}$) in these same experiments display a normal convergence with time (Fig. 5C and D). Because we infer that chrysotile–water and talc–water oxygen-isotope exchange by volume diffusion is much slower compared to hydrogen isotope exchange, it is reasonable to presume that lizardite behaves similarly. If that is the case, then oxygen-isotope exchange in the lizardite experiments was probably controlled solely by the conversion of lizardite to chrysotile, with the calculated extent of exchange being governed only by the degree of this phase transformation.

Table 3
Mineral–water fractionation factors.

Phase	T (°C)	^{18}O–^{16}O $1000\ln\alpha_{min-water}$	D–H $1000\ln\alpha_{min-water}$
Serpentine	250	3.1 ± 1.2[a]	-32 ± 15[b]
Serpentine	350	0.0 ± 1.1[a]	-29 ± 8[b]
Serpentine	450	-3.1 ± 1.3[b]	-20 ± 2[b]
Talc	250	6.5 ± 0.6[c]	-34 ± 7[c]
Talc	350	1.7 ± 0.6[c]	-33[c,d]
Talc	450	-0.4 ± 0.2[c]	-31 ± 4[c]

[a] Lizardite–water experiment.
[b] Chrysotile–water experiment.
[c] Talc synthesis experiment.
[d] Minimum value. See text for explanation.

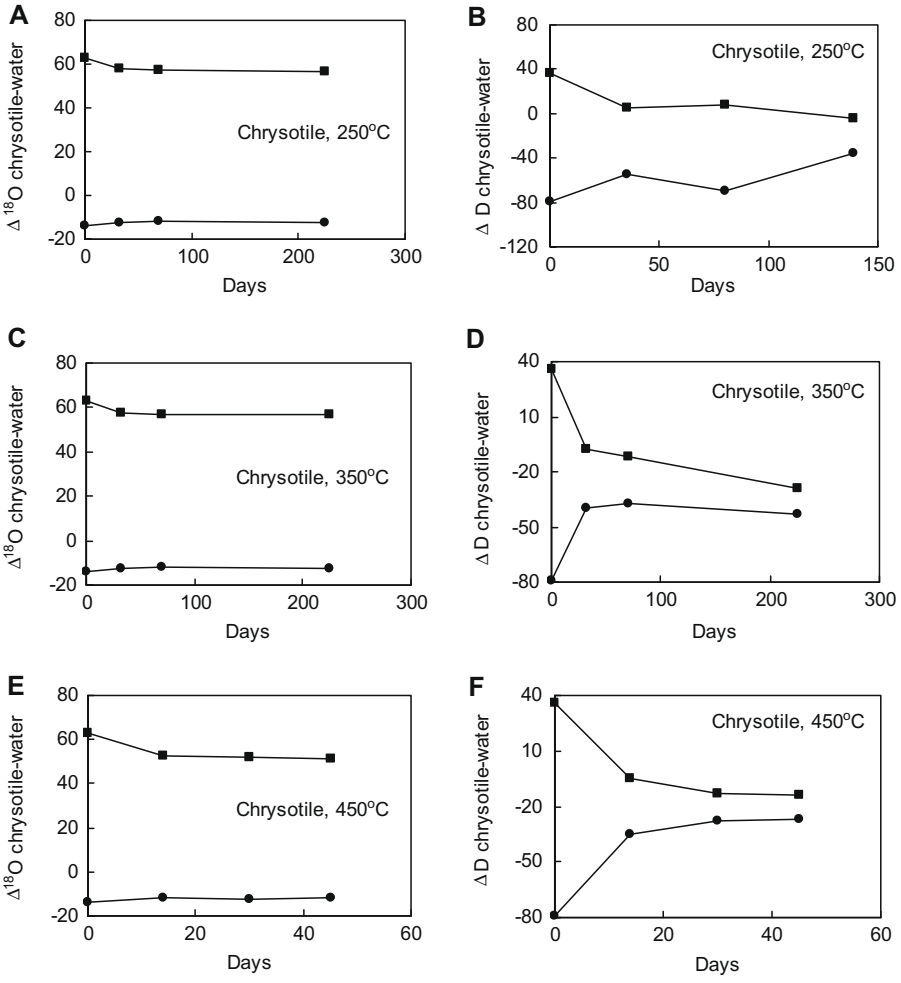

Fig. 4. Mineral–water fractionation ($\delta_{mineral} - \delta_{water}$) versus experimental run-time during the reaction of chrysotile and NaCl solutions from 250 to 450 °C. Individual graphs show data for companion runs involving isotopically enriched (circles) and depleted (squares) waters. Hydrogen isotope exchange varied from 73% to 89% from 250 to 450 °C, respectively. Oxygen-isotope exchange in these same experiments was minimal (<19%), as evidenced by mineral–water fractionation trends that converge only slightly with time.

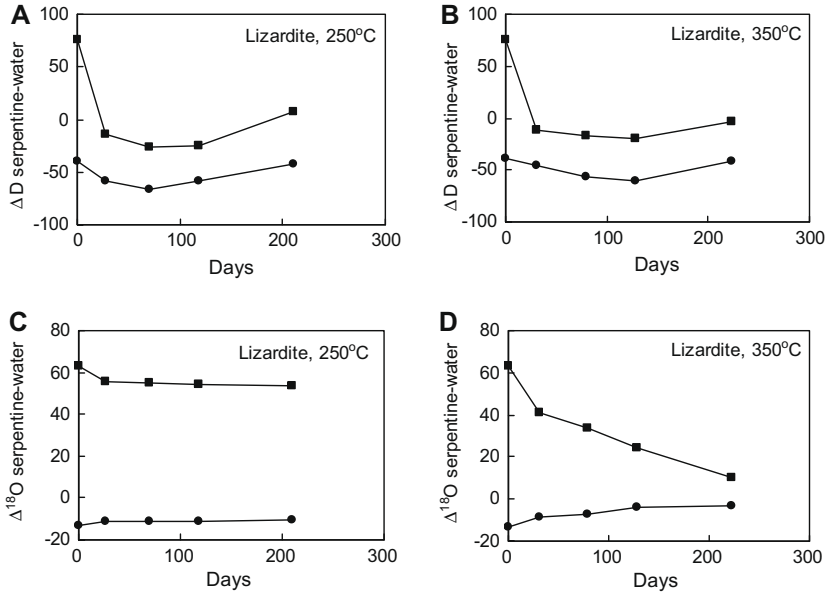

Fig. 5. Mineral–water fractionation ($\delta_{mineral} - \delta_{water}$) versus experimental run-time during the reaction of lizardite and NaCl solutions at 250 and 350 °C. Individual graphs show data for companion runs involving isotopically enriched (circles) and depleted (squares) waters. Oxygen-isotope exchange was facilitated by recrystallization of lizardite to chrysotile fibers as a function of time. Hydrogen isotope fractionation failed to converge with time in companion runs, possibly due to competing diffusion and recrystallization processes operating at different rates.

4. DISCUSSION

Talc–water and serpentine–water oxygen isotope fractionation have not been calibrated previously by experiment. Wenner and Taylor (1971) proposed a fractionation curve for serpentine based on $\delta^{18}O$ data for chlorites in metasedimentary rocks and the assumption that chlorite and serpentine partition ^{18}O similarly. The resulting fractionation curve was subsequently modified by O'Hanley (1996) and differs from those proposed by Savin and Lee (1988) and Zheng (1993) which are based on a semi-empirical model using correlations of cation–oxygen bond strengths in minerals as a function of ^{18}O enrichment in those same minerals. These latter two studies are also the only source of oxygen isotope fractionation factors for the talc–water system.

The ^{18}O–^{16}O fractionation factors for the talc–water system derived by experiment in this study are in good agreement with those predicted by the semi-empirical models of Zheng (1993) and Savin and Lee (1988) from 350 to 450 °C (Fig. 6). Our value at 250 °C, however, is larger by approximately 2‰, suggesting a larger dependence of the fractionation factor on temperature. Based on the experimental data reported here, talc–water ^{18}O–^{16}O fractionation can be described by the following regression as a function of temperature from 250 to 450 °C at 50 MPa:

$$1000ln\alpha^{^{18}O-^{16}O}_{talc-water} = 11.70 \times 10^6/T^2 - 25.49 \times 10^3/T + 12.48 \quad (5)$$

where T is temperature in Kelvin.

With respect to ^{18}O–^{16}O fractionation factors in the serpentine–water system, our new experimental data display an identical dependence on temperature compared to the predictions of Savin and Lee (1988) but are more positive

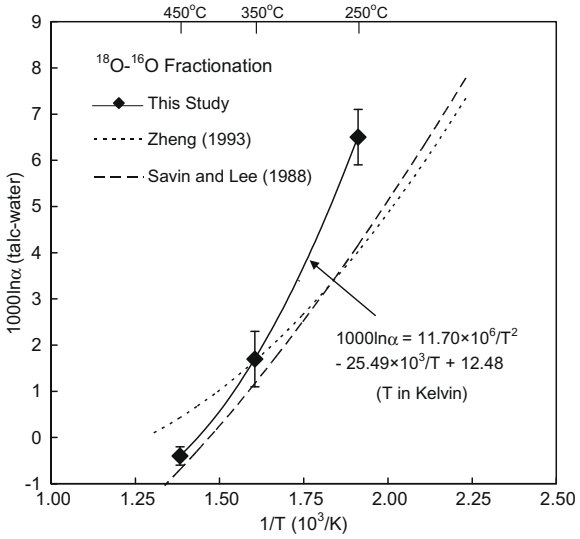

Fig. 6. ^{18}O–^{16}O fractionation factors (1000 lnα) in the talc–water system as a function of temperature. The experimental 1000 lnα values from this study decrease with increasing temperature in a non-linear fashion and are in good agreement with the theoretical predictions of Savin and Lee (1988) and Zheng (1993) at temperatures from 350 to 450 °C but are approximately 2‰ more positive at 250 °C.

by approximately 1‰ (Fig. 7). Our experimental point at 350 °C is also in excellent agreement with the predictions of Zheng (1993) and Wenner and Taylor (1971) as modified by O'Hanley (1996), but the smaller temperature dependence predicted by these prior studies yields values that are approximately 2‰ more negative and positive at 250 and 450 °C, respectively. A regression of our experimental

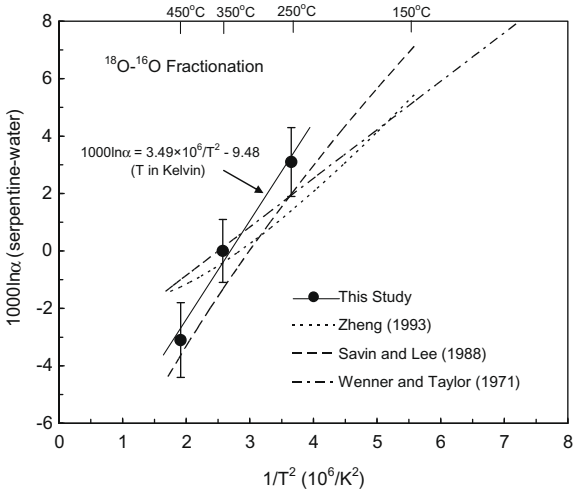

Fig. 7. ^{18}O–^{16}O fractionation factors (1000 lnα) in the serpentine–water system as a function of temperature. The experimental 1000 lnα values from this study decrease with increasing temperature and were linearly regressed from 250 to 450 °C. The resulting fractionation factors display a steeper dependence on temperature compared to the field-based prediction of Wenner and Taylor (1971), as modified by O'Hanley (1996), and the semi-empirical model of Zheng (1993), and are approximately 1‰ more positive than those computed by Savin and Lee (1988).

data as a function of temperature yields the following equation that can be used to describe serpentine–water ^{18}O–^{16}O fractionation from 250 to 450 °C, 50 MPa:

$$1000ln\alpha^{^{18}O-^{16}O}_{serpentine-water} = 3.49 \times 10^6/T^2 - 9.48 \quad (6)$$

where T is temperature in Kelvin. It should be noted that $\Delta^{18}O_{talc-serpentine}$ is weakly dependent on temperature at the conditions of these experiments, varying from 2.4‰ at 250 °C to 2.7‰ at 450 °C. Accordingly, talc–serpentine pairs do not appear to be a sensitive ^{18}O–^{16}O geothermometer over this temperature interval. Combining the experimental ^{18}O–^{16}O fractionation factors in the brucite–water system (Saccocia et al., 1998) with the data for serpentine–water reported here yields $\Delta^{18}O_{serpentine-brucite}$ values that vary from −2.9 to +0.8‰ from 250 to 450 °C, respectively. This variation may provide enough analytical resolution to use serpentine–brucite pairs in altered ultramafic rocks as an ^{18}O–^{16}O geothermometer.

Wenner and Taylor (1973) derived a D–H serpentine–water fractionation curve by integrating one experimental point for antigorite at 400 °C, 100 MPa (Suzuoki and Epstein, 1976) with D–H data from three natural serpentine samples, and assuming the temperature and isotopic composition of the water associated with serpentine formation. The resulting curve diverges significantly from the experimental calibration of serpentine–water D–H fractionation proposed by Sakai and Tsutsumi (1978). In particular, the Wenner and Taylor (1973) curve predicts that serpentine should be progressively more depleted in D compared to the water from which it precipitates with decreasing temperature, whereas the experimental data of Sakai and Tsutsumi (1978) yields the opposite relationship. The discrepancy is relatively small at 400 °C (7‰) but increases to nearly 150‰ at 25 °C, which makes interpretation of the D–H composition of natural serpentine highly equivocal.

A comparison of the experimental D–H serpentine–water fractionation factors determined here with these previous studies reveals good agreement with the field-based calibration of Wenner and Taylor (1973) and the single experimental point of Suzuoki and Epstein (1976) at 400 °C, 100 MPa (Fig. 8). Compared to the experimental calibration of Sakai and Tsutsumi (1978) at 200 MPa, our values at 50 MPa are more negative by 7–26‰ from 450 to 250 °C, respectively. Theoretical models and experimental calibrations do indicate that increasing pressure increases hydrogen isotope fractionation factors in mineral–water systems (Driesner, 1997; Horita et al., 1999, 2002). In the brucite–water system, for example, the hydrogen isotope fractionation factor increases by approximately 4‰ at 450 °C as pressure increases from 50 to 200 MPa, with smaller increases (<3‰) observed over this same pressure interval at lower temperature (Horita et al., 2002). Because this observed pressure-effect has been attributed largely to the pressure-dependent properties of water and not the mineral (Horita et al, 2002), it is reasonable to assume that it also applies to the serpentine–water system. Thus, pressure differences could account for over half of the observed discrepancy of our experimental point at 450 °C, 50 MPa with that of Sakai and Tsutsumi (1978) at 200 MPa, yielding reasonably good agreement. However, the relatively small pressure-effect of <3‰ from 50 to

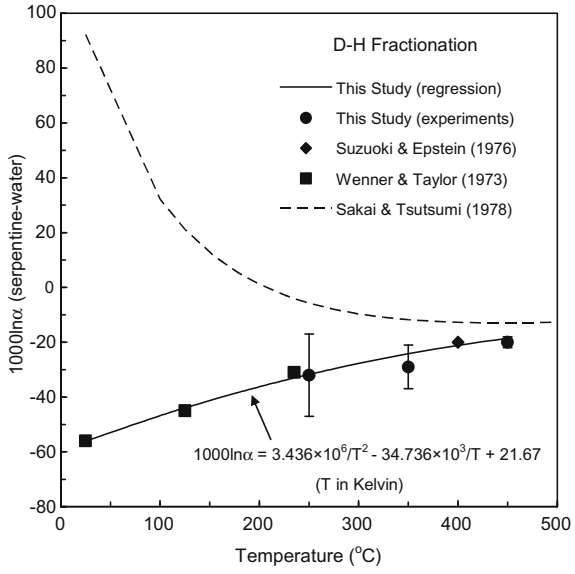

Fig. 8. D–H fractionation factors (1000 lnα) in the serpentine–water system as a function of temperature. Our experimental data from 250 to 450 °C, 50 MPa, form a consistent trend with the single experimental point at 400 °C, 100 MPa (Suzuoki and Epstein, 1976) and field-calibrated points at temperatures less than 250 °C (Wenner and Taylor, 1973). These data were adjusted for the pressure-effect and regressed to describe serpentine–water fractionation from 25 to 450 °C at 50 MPa. The previous experimental work of Sakai and Tsutsumi (1978) at 200 MPa is in reasonable agreement with our 450 °C data if pressure differences are considered. At lower temperatures, the pressure-effect on hydrogen isotope fractionation cannot account for the observed discrepancies.

200 MPa cannot account for the much larger difference in measured fractionation factors (up to 26‰) at lower temperatures.

Mineev and Grinenko (1996) report D–H fractionation factors for the serpentine–water system at 100 and 200 °C and at 0.1 and 250 MPa, however no details about the experimental methodology employed were provided. Based on their results, they proposed that the large temperature-dependent discrepancy between the Wenner and Taylor (1973) and Sakai and Tsutsumi (1978) calibrations could indeed be attributed to differences in pressure. This conclusion, however, does not appear to be consistent with theoretical and experimental calibrations of the pressure-effect on hydrogen isotope fractionation when the field-context of the natural samples used by Wenner and Taylor (1973) is also considered.

Wenner and Taylor (1973) used two oceanic serpentine samples dredge from the Mid-Atlantic Ridge to anchor their serpentine–water D–H fractionation curve from 125 to 235 °C. A serpentine–magnetite oxygen-isotope geothermometer (Wenner and Taylor, 1971) was used to constrain temperature of formation. Serpentine–water fractionation factors were then computed from the measured δD of the serpentine along with the assumption that the serpentine equilibrated with hydrothermal solutions having a δD equivalent to that of seawater. Although it is likely that the serpentinized ultramafic rocks used for this analysis were altered below the seafloor (based on the temperatures), a water depth of 3000 m indicates that a seafloor pressure of approximately 30 MPa in this ridge environment can be adopted as a minimum pressure for serpentine–water equilibration. Thus, a comparison of the fractionation factors proposed by Wenner and Taylor (1973) with those of Sakai and Tsutsumi (1978) requires a pressure correction from 30 to 200 MPa at relatively low temperature. At these conditions, the pressure-effect is less than 5‰ (Horita et al, 2002), and would be smaller if the serpentinized ultramafic rocks were altered below the seafloor at pressures greater than 30 MPa. Thus, the 25–60‰ discrepancy between the Wenner and Taylor (1973) and Sakai and Tsutsumi (1978) fractionation factors from 235 to 125 °C is impossible to account for by the pressure-effect alone.

Our new experimental points at 250, 350, and 450 °C, 50 MPa, and the 400 °C, 100 MPa experimental point from Suzuoki and Epstein (1976), together with the three low temperature (<250 °C, 30 MPa estimate) field-based points proposed by Wenner and Taylor (1973) define a single systematic trend of D–H serpentine–water fractionation as a function of temperature (Fig. 8). We have used these data to refine and extend the original fractionation curve proposed by Wenner and Taylor (1973) to describe D–H serpentine–water fractionation from 25 to 450 °C at 50 MPa. Applying the pressure correction to the Suzuoki and Epstein (1976) and Wenner and Taylor (1973) data and regressing the results to create a consistent 50 MPa fractionation curve yields the relationship:

$$1000ln\alpha^{D-H}_{serpentine-water} = 3.436 \times 10^6/T^2 - 34.736 \times 10^3/T + 21.67 \quad (7)$$

where T is temperature in Kelvin. This new fractionation curve is not consistent with that proposed by Sakai and Tsutsumi (1978) at low temperature and we have no explanation for this discrepancy. Because the curve proposed here is based on consistent experimental measurements *and* field-based observations over a large temperature range, we believe that it more accurately describes the temperature dependence of D–H serpentine–water fractionation.

Our D–H fractionation factors in the talc–water and serpentine–water systems are shown in Fig. 9, for comparison with other hydrous minerals. The micas and hornblende all display a consistent and systematic dependence on temperature, characterized by fractionation factors decreasing with temperature. In contrast, the fractionation factor for talc is only weakly dependent on temperature from 250 to 450 °C, similar to brucite over this same temperature interval (Satake and Matsuo, 1984; Saccocia et al., 1998). Chlorite also displays this same behavior from 500 to 700 °C (Graham et al. 1984) and has a D–H fractionation trend that approaches our data for talc at 450 °C. Our experimental D–H fractionation factors for the talc–water system at 250–450 °C, 50 MPa, can be described by the following relationship:

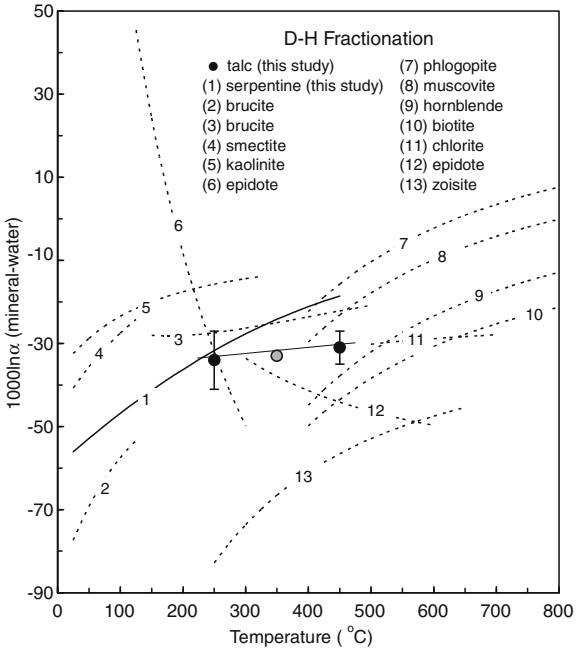

Fig. 9. D–H fractionation factors for hydrous minerals as a function of temperature. The fractionation factors for talc reported here were linearly regressed from 250 to 450 °C and the result shows a weak dependence on temperature, similar to brucite and chlorite. Our refined D–H fractionation trend for serpentine (curve 1) is also shown for comparison with other phases. References are as follows: (2) Xu and Zheng (1999), (3) Satake and Matsuo (1984), (4) Yen (1980), (5) Gilg and Sheppard (1996), (6, 13) Graham et al. (1980), (7, 8, 9, 10) Suzuoki and Epstein (1976), (11) Graham et al. (1984), (12) Chacko et al. (1999).

$$1000ln\alpha^{D-H}_{talc-water} = 10.88 \times 10^6/T^2 - 41.52 \times 10^3/T + 5.61 \quad (8)$$

where T is temperature in Kelvin. Because of the differences in temperature-dependent D–H fractionation, brucite–serpentine and talc–serpentine pairs could be used as a geothermometer in serpentinized rocks, if equilibrium isotope fractionation is assumed. For example, D–H fractionation for talc–serpentine varies from −2 to −11‰ from 250 to 450 °C, 50 MPa based on the experimental data reported here.

Results of this study have important implications for our understanding of serpentine formation, particularly in the oceanic lithosphere at mid-ocean ridges where serpentine typically has negative δD values (Früh-Green et al, 2004 and references therein). Based on the fractionation curve of Sakai and Tsutsumi (1978), these negative values would imply serpentine formation from hydrothermal fluids that are strongly depleted in deuterium relative to seawater. This result, if correct, would suggest greater involvement of magmatic waters or perhaps a more evolved reaction path involving seawater. Our new experimental results affirm the idea that hydrothermal fluids involved in serpentine formation have more positive δD values, closer to that of seawater. However, it should be emphasized that our serpentine–water and talc–water D–H fractionation curves can only be used to model natural systems where any pressure-effect would be minimal. Within the mid-ocean ridge environment, circulating hydrothermal fluids can attain temperature and pressure conditions that approach the critical point of seawater. At these extreme conditions, the D–H fractionation factor in mineral–water systems may change dramatically with relatively small changes in temperature and pressure (Horita et al., 2002). Reaction path modeling of ultramafic rock–seawater interaction could clarify the significance of this effect on the isotopic composition of serpentinites.

5. CONCLUSIONS

Oxygen and hydrogen isotope fractionation in the talc–water and serpentine–water systems was measured by experiment from 250 to 450 °C at 50 MPa. Talc recrystallization is kinetically inhibited over this temperature range, preventing extensive exchange of oxygen- and hydrogen-isotopes with a coexisting aqueous phase. Isotope exchange was, however, nearly 100% during the synthesis of talc from an initial brucite + quartz assemblage at 350 and 450 °C. Based on the results of talc synthesis experiments, we report the first experimental calibration of ^{18}O–^{16}O and D–H fractionation in the talc–water system. Our results indicate that ^{18}O–^{16}O talc–water fractionation decreases with increasing temperature from 6.5 ± 0.6 to -0.4 ± 0.2‰ from 250 to 450 °C, respectively. For D–H isotopes, the talc–water system displays a very weak dependence on temperature with fractionation factors varying from -34 ± 7 to -31 ± 4‰ from 250 to 450 °C, respectively. The weak temperature dependence is similar to that displayed by experimental results in the brucite–water and chorite–water systems, but is quite distinct from the behavior noted for other hydrous silicates such as hornblende and micas.

In the serpentine–water system, oxygen isotope exchange was enhanced by both increasing temperature and the recrystallization of lizardite to chrysotile. The ^{18}O–^{16}O serpentine–water fractionation factor decreases with increasing temperature from 3.1 ± 1.2‰ at 250 °C to -3.1 ± 1.3‰ at 450 °C. Based on previous work in the brucite–water system (Saccocia et al, 1998), serpentine–brucite represents a potential ^{18}O–^{16}O geothermometer characterized by a $\Delta^{18}O_{serpentine-brucite}$ value that varies by approximately 4‰ over the 200°C temperature interval investigated here. Serpentine–water D–H fractionation factors reported here from experiments decrease with temperature from -20 ± 2‰ at 450°C to -32 ± 15‰ at 250 °C, and are consistent with the low temperature (<250 °C) field-calibrated fractionation factors reported by Wenner and Taylor (1973). The effect of pressure on hydrogen isotope fractionation can account for the relatively small discrepancy between the serpentine–water fractionation factor reported here at 450 °C, 50 MPa and the value from Sakai and Tsutsumi (1978) at 200 MPa. However, the pressure-effect is too small at lower temperatures within this pressure range to account for the much larger discrepancy observed at those conditions. This result indicates that serpentine incorporates less deuterium in its crystal structure compared to the coexisting aqueous phase at progressively lower temperature and confirms that natural serpentine samples with negative δD values from mid-ocean ridge environments likely form by interaction with hydrothermal fluids having a δD similar to seawater. Fractionation of hydrogen isotopes between coexisting talc and serpentine varies by 9‰ from 250 to 450 °C, 50 MPa, suggesting that talc–serpentine pairs could be used as a D–H geothermometer if isotopic equilibrium between the two phases is maintained.

ACKNOWLEDGMENTS

This work was supported by NSF Grants OCE-9313980 to the Woods Hole Oceanographic Institution and OCE-9820287 to Bridgewater State College (BSC). Thoughtful reviews by Craig Johnson and Robert Seal prior to submission and comments by Gretchen Früh-Green and two anonymous reviewers helped to improve the manuscript. We are also indebted to the Royal Ontario Museum and the Calidria Asbestos Company for donating mineral samples used in these experiments. Finally, the assistance of former BSC students Karen Hurley and Daniel DeSousa in the laboratory is also appreciated.

REFERENCES

Berman R. G. (1988) Internally-consistent thermodynamic data for minerals in the system Na_2O–K_2O–CaO–MgO–FeO–Fe_2O_3–Al_2O_3–SiO_2–TiO_2–H_2O–CO_2. *J. Petrol.* **29**, 445–522.

Blackman D. K., Cann J. R., Jenesen B. and Smith D. K. (1998) Origin of extensional core complexes: evidence from the Mid-Atlantic Ridge at atlantis fracture zone. *J. Geophys. Res.* **103**, 21315–21333.

Chacko T., Cole D. R. and Horita J. (2001) Equilibrium oxygen, hydrogen, and carbon isotope fractionation factors applicable

to geologic systems. In *Stable Isotope Geochmistry*, vol. 43 (eds. D. R. Cole and J. W. Valley). Min. Soc. Amer., pp. 1–81.

Chacko T., Riciputi L. R., Cole D. R. and Horita J. (1999) A new technique for determining equilibrium hydrogen isotope fractionation factors using the ion microprobe: application to the epidote–water system. *Geochim. Cosmochim. Acta* **63**, 1–10.

Clayton R. N. and Mayeda T. K. (1963) The use of bromine pentafluoride in the extraction of oxygen in oxides and silicates for isotopic analysis. *Geochim. Cosmochim. Acta* **27**, 43–52.

Cole D. R. and Ohmoto H. (1986) Kinetics of isotopic exchange at elevated temperatures and pressures. In *Stable Isotopes in High Temperature Geologic Processes*, vol. 16 (eds. J. W. Valley, H. P. Taylor and J. R. O'Neil). Min. Soc. Amer., pp. 41–90.

Coleman M. L., Shepherd T. J., Durham J. J., Rouse J. E. and Moore G. Z. R. (1982) Reduction of water with zinc for hydrogen isotope analysis. *Anal. Chem.* **54**, 993–995.

Driesner T. (1997) The effect of pressure on deuterium–hydrogen fractionation in high-temperature water. *Science* **277**, 791–794.

Driesner T. and Seward T. M. (2000) Experimental and simulation study of salt effects and pressure/density effects on oxygen and hydrogen stable isotope liquid–vapor fractionation for 4–5 molal aqueous NaCl and KCl solutions to 400 °C. *Geochim. Cosmochim. Acta* **64**, 1773–1784.

Escartin J. G., Hirth G. and Evans B. (1997) Nondilatant brittle deformation of serpentinites: implications for Mohr–Coulomb theory and the strength of faults. *J. Geophys. Res.* **102**, 2897–2913.

Früh-Green G. L., Connolly J. A. D., Plas A., Kelley D. S. and Grobéty B. (2004) Serpentinization of oceanic peridotites: implications for geochemical cycles and biological activity. In *The Subseafloor Biosphere at Mid-Ocean Ridges* (eds. W. S. D. Wilocock, E. F. DeLong, D. S. Kelley, J. A. Baross and S. C. Cary). American Geophysical Union, Washington D.C., pp. 119–136.

Gilg H. A. and Sheppard S. M. F. (1996) Hydrogen isotope fractionation between kaolinite and water revisited. *Geochim. Cosmochim. Acta* **60**, 529–533.

Godfrey J. D. (1962) The deuterium content of hydrous minerals from the East-Central Sierra Nevada and Yosemite National Park. *Geochim. Cosmochim. Acta* **26**, 1215–1245.

Graham C. M., Sheppard S. M. F. and Heaton T. H. (1980) Experimental hydrogen isotope studies I. Systematics of hydrogen isotope fractionation in the systems epidote–H_2O, zoisite–H_2O, and AlO(OH)–H_2O. *Geochim. Cosmochim. Acta* **44**, 353–364.

Graham C. M., Atkinson J. and Harmon R. S. (1984) Hydrogen isotope fractionation in the system chlorite–water. NERC 6th Progress Report 1981–1984, NERC Publication Series D. No. 25, pp. 139.

Hirth G., Escartin J. and Lin J. (1998) The rheology of the lower oceanic crust: implications for lithospheric deformation at mid-ocean ridges. In *Faulting and Magmatism at Mid-Ocean Ridges* (eds. W. R. Buck, P. T. Delaney, J. A. Karson and Y. Lagabrielle), vol. 106, pp. 291–303.

Horita J., Cole D. R. and Wesolowski D. (1995) The activity-composition relationship of oxygen and hydrogen isotopes in aqueous salt-solutions: III. Vapor–liquid water equilibration of NaCl solutions to 350 °C. *Geochim. Cosmochim. Acta* **59**, 1139–1151.

Horita J., Driesner T. and Cole D. R. (1999) Pressure effect on hydrogen isotope fractionation between brucite and water at elevated temperatures. *Science* **286**, 1545–1547.

Horita J., Cole D. R., Polyakov V. B. and Driesner T. (2002) Experimental and theoretical study of pressure effects on hydrogen isotope fractionation in the system brucite–water at elevated temperatures. *Geochim Cosmochim. Acta* **66**, 3769–3788.

Kelley D. S., Karson J. A., Blackman D. K., Früh-Green G. L., Buttefield D. A., Lilley M. D., Olson E. J., Schrenk M. O., Roe K. K., Lebon G. T., Rivizzigno P. and the AT3-60 Shipboard Party (2001) An off-axis hydrothermal vent field near the Mid-Atlantic Ridge at 30°N, Nature 412, 145–149.

Kelso, R. R., Richter C. and Pariso J. E. (1996) Rock magmatic properties, magnetic mineralogy, and paleomagnestism of peridotites from Hess Deep. In *Proceedings of the Ocean Drilling Program Scientific Results* (eds. C. Mevel, K. M. Gillis, J. F. Allan and P. S. Meyer), vol. 147, pp. 405–413.

Matthews A., Goldsmith J. R. and Clayton R. (1983) On the mechanisms and kinetics of oxygen isotope exchange in quartz and feldspars at elevated temperatures and pressures. *Geol. Soc. Amer. Bull.* **94**, 396–412.

Mevel C. and Cannat M. (1992) Lithospheric stretching and hydrothermal processes in oceanic gabbros from slow spreading ridges. In *Ophiolite Genesis and Evolution of the Oceanic Lithosphere*. Kluwer Acad, pp. 293–312.

Miller D. J., Iturrino G. J. and Chistensen N. I. (1996) Geochemical and petrological constraints on the velocity behavior of lower crustal and upper mantle rocks from the fast-spreading ridge at Hess Deep. In *Proceedings of the Ocean Drilling Program Scientific Report* (eds. C. Mevel, K. M. Gillis, J. F. Allan and P. S. Meyer), vol. 147, pp. 477–490.

Mineev S. D. and Grinenko V. A. (1996) The pressure influence on hydrogen isotopes fractionation in the serpentine–water system. V M Goldschnidt Conf. Abstr. 1, 404.

Northrop D. A. and Clayton R. N. (1966) Oxygen isotope fractionations in systems containing dolomite. *J. Geol.* **74**, 174–196.

O'Hanley D. S. and Dyar M. D. (1993) The composition of lizardite 1T and the formation of magnetite in serpentinites. *Amer. Min.* **78**, 391–404.

O'Hanley D. S. (1996) *Serpentinites: Records of Tectonic and Petrological History*. Oxford Univ. Press, New York.

O'Neil J. R., Adami L. H. and Epstein S. (1975) Revised value for the ^{18}O fractionation between CO_2 and water at 25 °C. *U.S. Geol. Surv. J. Res.* **3**, 623–624.

Saccocia P. J. and Seyfried, Jr., W. E. (1990) Talc–quartz equilibria and the stability of magnesium chloride complexes in NaCl–$MgCl_2$ solutions at 300, 350, and 400 °C, 500 bars. *Geochim. Cosmochim. Acta* **54**, 3283–3294.

Saccocia P. J., Seewald J. S. and Shanks, III, W. C. (1998) Hydrogen and oxygen isotope fractionation between brucite and aqueous NaCl solutions from 250–450 °C. *Geochim. Cosmochim. Acta* **62**, 485–492.

Sakai H. and Tsutsumi M. (1978) D/H fractionation factors between serpentine and water at 100 to 500 °C and 2000 bar water pressure, and the D/H ratios of natural serpentines. *Earth Planet. Sci. Lett.* **40**, 231–242.

Satake H. and Matsuo S. (1984) Hydrogen isotope fractionation factor between brucite and water in the temperature range from 100 up to 500 °C. *Contrib. Mineral. Petrol.* **86**, 19–24.

Savin S. M. and Lee M. (1988) Isotopic studies of phyllosilicates. In *Hydrous Phyllosilcates (excusive of micas)* (ed. S. W. Bailey). *Rev. Mineral.* 19, pp. 189–223.

Suzuoki T. and Epstein S. (1976) Hydrogen isotope fractionation between OH-bearing minerals and water. *Geochim. Cosmochim. Acta* **40**, 1229–1240.

Wenner D. B. and Taylor, Jr., H. P. (1971) Temperatures of serpentinization of ultramafic rocks based on O^{18}/O^{16} fractionation between coexisting serpentine and magnetite. *Contr. Mineral. Petrol.* **32**, 165–185.

Wenner D. B. and Taylor, Jr., H. P. (1973) Oxygen and hydrogen isotope studies of the serpentinization of ultramafic rocks in oceanic environments and continental ophiolite complexes. *Am. J. Sci.* **273**, 207–239.

Xu B.-L. and Zheng Y.-F. (1999) Experimental Studies of oxygen and hydrogen isotope fractionations between precipitated brucite and water at low temperatures. *Geochim. Cosmochim. Acta* **63**, 2009–2018.

Yen H. (1980) D/H ratios and late-stage dehydration of shales during burial. *Geochim. Cosmochim. Acta* **44**, 341–352.

Zheng Y.-F. (1993) Calculation of oxygen isotope fractionation in hydroxyl-bearing silicates. *Earth Planet. Sci. Lett.* **120**, 247–263.

Zheng Y.-F. (1998) Oxygen isotope fractionation between hydroxide minerals and water. *Phys. Chem. Mineral.* **25**, 213–221.

Associate editor: Miryam Bar-Matthews